University of Twente

EEMCS / Electrical Engineering
Robotics and *Mechatronics*

Characterization, Modeling and Control of Magnetic Microrobots

H. (Hans) Kolk

BSc Report

Committee:
Dr. S. Misra
I.S.M. Khalil, PhD
Dr.ir. G. Koster

August 2013

Report nr. 023RAM2013
Robotics and Mechatronics
EE-Math-CS
University of Twente
P.O. Box 217
7500 AE Enschede
The Netherlands

Characterization, Modeling and Control of Magnetic Microrobots

Hans Kolk, Islam S.M. Khalil and Sarthak Misra
University of Twente, The Netherlands

***Abstract*— This work addresses the characterization, modeling and control of magnetic microrobots under the influence of the applied magnetic fields. The aim of this work is to investigate the motion characteristics (boundary frequency and velocity) of three microrobotic structures and control their position and orientation in two dimensions (2D). The microrobots used have rectangular, ellipsoid and diamond shapes with dimensions ranging from 25 $\times$ 100 µm to 50 $\times$ 500 µm. All microrobots contain a layer of ferromagnetic material ($Co_{80}Ni_{20}$) for propulsion and steering purposes. Thrust force is generated by magnetic field gradients, whereas torque is generated by the magnetic fields. The magnetic fields are generated by a planar magnetic system which is capable of generating fields of 52.5 mT and field gradients of 1.31 T/m in magnitude.**

I. INTRODUCTION

Microrobots can be used for different purposes, for instance, in minimally invasive surgery (MIS). MIS aims at reducing patient trauma and recovery time. Localized drug delivery in cancer treatment using microrobots is one subject of MIS that is being investivated [1]. This localisation could result in reduced side-effects since drugs will only affect diseased cells. Another advantage of microrobotic drug delivery is the possibility to deliver at hard-to-reach regions in the human body [2]. Another example of microrobots used in MIS is the OctoMag system, which is capable of retinal surgery in the eye using a magnetically controlled microrobot.

In order to investigate the use of microrobots for clinical purposes we aim to characterize and control a range of microrobots. This range consists of microrobots with ellipsoid, diamond and rectangular structure and varying lengts and widths. A model of the forces and torques acting on the microrobots microrobots and generated by setup has been developed. Using this model the required currents have been determined for an existing tracking and control system. Experiments are conducted on a magnetic system using four electromagnets and a microscope vision system for tracking. The controller is applied to this system to compare the developed model of the microrobots with the closed-loop control results. In order to devise a suitable microrobot structure, experiments are carried out on different microrobot structures. A performance index is deviced in terms of the microrobot linear and rotational velocity and drag. Based on this index the most suitable structure is selected.

The results of this project are: First a performance index for rotational and linear performance of different microrobot structures. Second a control system by which the position and orientation of the microrobot can be controlled using electromagnets for steering and driving. Combining this makes it possible to control three degrees-of-freedom (DOF) of the most suitable microrobot, i.e., two planar DOF and one rotational DOF using magnetic force and torque at a distance, respectively.

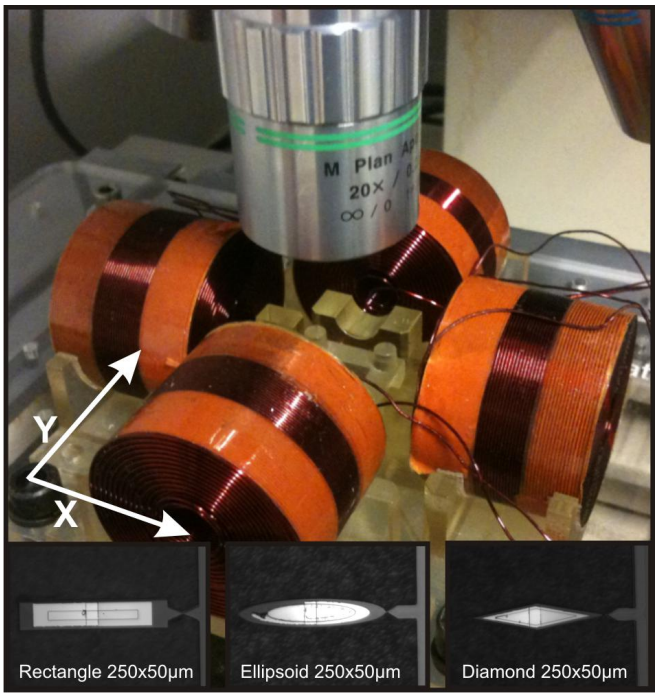

Fig. 1. Overview of the electromagnetic system. Four coils surround the work space which can be viewed through an optical microscope. The inset shows three microrobots fixed to their substrates.

II. CONTRIBUTIONS

During this project the following contributions are made:

- Characterisation of magnetic fields in the setup and increasing the magnetic field gradient through iron cores.
- Devising and calculation of a Performance Index for different microrobots.
- Characterisation of magnetic and drag forces and torques acting on the different microrobots.
- Determination of the boundary frequenciy of 18 different microrobots.
- Experiments to find linear velocity for 18 different microrobots.
- Creating feature tracking software for linear velocity experiments.
- Closed-Loop Control experiments of 9 different microrobots.

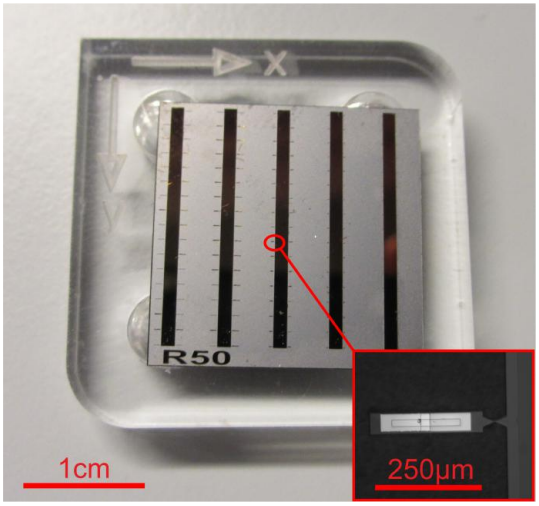

Fig. 2. A chip with 190 rectangular microrobots of width 50 µm and lengths varying from 50 to 500 µm. In the inset a magnification can be seen of one particular microrobot on the chip, as seen through the microscope.

III. MODELING OF MICROROBOTS

Control of the microrobots orientation and position requires both rotational and linear drag forces to be overcome by magnetic torque and magnetic field gradient, respectively. In this section the modeling of the friction torque and force will be discussed as well as the modeling of the magnetic torque and force generated by the magnetic system. First we will discuss the structures of the microrobots and the magnetic layer. Next the modeling of torques and forces will be discussed. Finally the setup will be discussed to show the magnetic fields and gradients that can be applied.

A. Microrobotic structures

The microrobots used for this project are a range of different sizes and shapes made of silicon nitride using photolithography techniques. A magnetic layer ($Co_{80}Ni_{20}$) is deposited on the microrobots for control purposes. The shapes used are ellipsoid, diamond and rectangular, as can be seen in figure 1. One chip contains 190 rectangular, ellipsoid or diamond shaped robots with a width of 25 or 50 µm and lengths varying from 50 to 500 µm. Such a chip measures 2 × 2 cm and can be seen in figure 2. All dimensions of the microrobots that are used can be seen in I.

TABLE I
DIMENSIONS OF THE MICROROBOTS AND THE MAGNETIC LAYERS, CORRESPONDING TO FIGURE 3.

Microrobot Lengths (L)	100 m	250 m	500 m
Magnetic Layer Lengths (Lmag)	60 m	150 m	300 m
Microrobot Widths (W)	25 m	50 m	
Magnetic Layer Widths (Wmag)	15 m	30 m	
Microrobot Thickness	2 m		
Magnetic Layer Thickness	0,2 m		

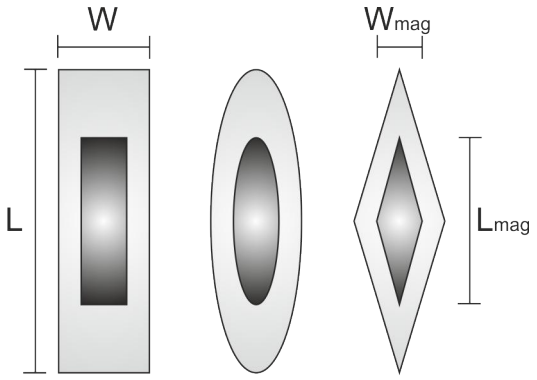

Fig. 3. Dimensions of the microrobots and the magnetic layers. W and L are the width and length of the microrobots whereas W_{mag} and L_{mag} are the width and length of the magnetic layer, respectively. These correspond with the values in table I.

B. Torque calculation

The rotational drag force can be calculated assuming Stokes drag. This assumption is valid because of the low Reynolds number at this scale. The drag torque is given by

$$T_d = -c_d\omega, \tag{1}$$

where T_d is the in-plane drag torque on the microrobot, ω is the angular velocity of the microrobot and c_d is the Stokes rotational drag coefficient. We can find this coefficient using a model for drag on an ellipsoid body, which is given by [3]

$$c_d = \frac{8\pi\gamma a^3}{3ln(2\frac{a}{b}) - \frac{1}{2}}, \tag{2}$$

where γ is the viscocity of water at room temperature and atmospheric pressure ($10^{-3}\mathrm{Kgm^{-1}s^{-1}}$ and a and b are half the length and width of the microrobot respectively.

In order to change the microrobots orientation, i.e. rotate the microrobot, the drag torque must be overcome by magnetic torque. A rotating external magnetic field is applied to create sufficient magnetic torque on the microrobot, see figure 4. The in-plane magnetic torque (T_m) is given by

$$T_m(\mathbf{P}) = |\mathbf{m} \times \mathbf{B}(\mathbf{P})|, \tag{3}$$

where $\mathbf{m}$ is the magnetic dipole moment of the microrobot, and $\mathbf{B}(\mathbf{P})$ is the applied magnetic field. The boundary frequency (f_b) is the lowest rotation frequency of the magnetic field at which the magnetic torque can no longer overcome the drag torque.

The different shaped microrobots also have different shapes of magnetic material layers on them. The magnetic layer is composed of a cobalt nickel alloy ($Co_{80}Ni_{20}$). The shape of this layer is of influence on the magnetization of the microrobots. Using a numerical method we calculated the magnetization factors $\mathrm{n_a}$ and $\mathrm{n_b}$ and use the following formula to calculate the generated magnetic torque [5] [6]

$$T_m = (n_a - n_b)\frac{1}{2}\mu_0 M_s^2 V, \tag{4}$$

where μ_0 is the permeability in vacuum ($4\pi \cdot 10^{-7}\mathrm{JA^{-2}m^{-1}}$), M_s is the saturation magnetisation

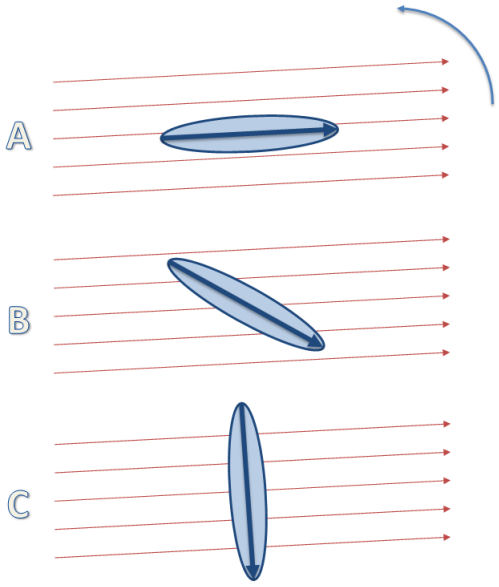

Fig. 4. Schematic view of the orientation of microrobot and the applied magnetic field with a counterclockwise rotation frequency. At low frequencies (A) the microrobot is aligned with the magnetic field, at higher frequencies (B) a phase shift between the microrobot and the magnetic field appears and at the boundary frequency (C) the microrobot and the magnetic field are oriented perpendicular.

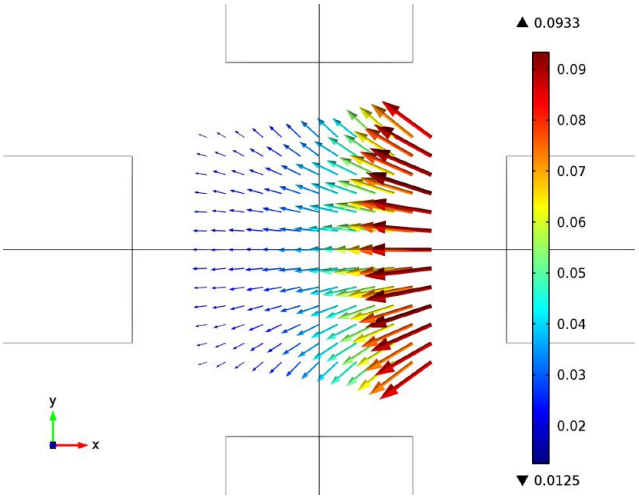

Fig. 5. This figure shows a finite element analyses of the magnetic field in the center of the setup. One coil (right) is active, to which a current of 1 A is supplied. This results in maximum magnetic field gradient, which is desired to apply force to the microrobots. The maximum magnetic field in the workspace is 52.5 mT whereas the average magnetic field gradient is 1.31 T/m in magnitude. This figure shows magnetic field vectors for an area of 12 × 12 mm, the central 6 × 6 mm of this area covers the workspace. The values on the sidebar are in Tesla.

of $Co_{80}Ni_{20}$ ($1.19 \cdot 10^6 \mathrm{Am}^{-1}$). Further, V is the volume of the magnetic material on the microrobot and $(n_a - n_b)$ are the anisotropy factors.

C. Force calculation

Analoguous to the torque calculation, Stokes drag is assumed for the drag force. The drag force is given by the drag equation [7]

$$F_d = -\frac{1}{2}\gamma\rho v^2 A, \tag{5}$$

where F_d is the drag force on the microrobot, v is the microrobots linear velocity, γ is the drag coefficient, ρ is the density of the water and A is the surface of the microrobot on the water.

The drag force needs to be overcome by the magnetic force on the microrobot, which can be written as

$$F_m(\mathbf{P}) = |(\mathbf{m}\cdot\nabla)\mathbf{B}(\mathbf{P})|, \tag{6}$$

where $\mathbf{m}$ is the magnetisation of the microrobot and $\mathbf{B}(\mathbf{P})$ is the applied magnetic field. Magnetisation $(\mathbf{m})$ can be calculated as follows

$$|\mathbf{m}| = M_s V, \tag{7}$$

where M_s is the saturation magnetisation of $Co_{80}Ni_{20}$ ($1.19 \cdot 10^6 \mathrm{Am}^{-1}$) and V is the volume of the magnetic material on the microrobot.

D. Magnetic System

The magnetic system that is used for this project is a two dimensional (2D) setup, with a top view camera mounted on a microscope for vision. There are four coils in order to generate magnetic fields. In order to enlarge the magnetic fields and gradients we devised iron cores of 70 mm long and 5 mm diameter. These were used during the control experiments as well as during linear velocity characterization experiments.

A finite element analyses of the setup has been done to find the magnetic fields and field gradients in the area of interest. For this the program Comsol Multiphysics has been used. Using this program a model of the copper coils with iron cores has been made. The area of interest is the workspace of the reservoir, which has a diameter of 6 mm. A graphical representation of the magnetic field can be seen in figure 6. Here a current of 1A is supplied to one core, in order to generate the largest magnetic field gradient. From the Comsol simulation we find the magnetic fields at points in the workspace. The maximum field strength in the workspace is 52.5 mT in magnitude. Using this data we can create a polynomial fit of the magnetic field which allows for calculating the magnetic field gradient. The average of the magnetic field gradient in the direction of the active coil is 1.31 T/m in magnitude.

E. Characterization: Performance Index

For linear motion a performance index based on the magnetic-Richardson number (Ψ_l) quantifies the ratio between the applied magnetic forces and the drag forces that the water exerts on the microrobot.[4] We define it as the ratio:

$$\Psi_l = \frac{\text{Magnetic force on microrobot}}{\text{Stokes drag force on microrobot}} = \frac{F_m}{F_d}. \tag{8}$$

A similar performance index is devised for rotation (Ψ_r) which quantifies the ration between applied magnetic torque

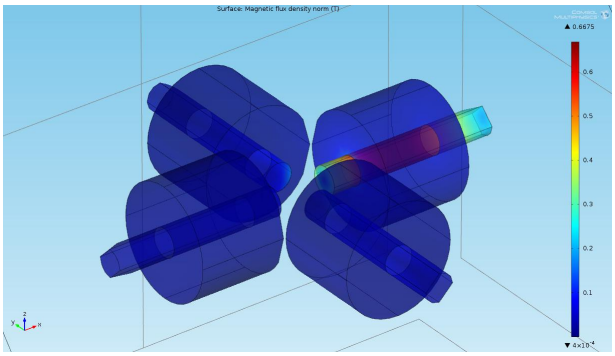

Fig. 6. This figure shows the Comsol model of the coils and cores that is used to evaluate the magnetic fields and gradients in the setup.

and the drag torque on the microrobot:

$$\Psi_r = \frac{\text{Magnetic torque on microrobot}}{\text{Stokes drag torque on microrobot}} = \frac{T_m}{T_d}. \quad (9)$$

IV. EXPERIMENTAL WORK

In this section the procedure and results of the experimental work is discussed. First the rotational experiments are discussed, which were carried out to calculate the Rotational Richardson Number. Second the linear experiments are discussed, to find the Linear Richardson Number. Third the tracking system is discussed. Finally Closed-Loop Control experiments are done for several microrobots.

A. Rotational Boundary Frequency Experiments

The Rotational Boundary Frequency has been determined for all microrobots. The boundary frequency is the maximum rotation frequency at which the microrobot can follow the direction of the magnetic field, see figure 4. Above the boundary frequency the microrobot starts turning back and forth in both directions. The experiments are conducted using an input current of 0.3 A, without metal cores in the coils. This current is the highest at which it is still possible to find the boundary frequency. Using a higher field it is no longer possible to detect this due to the limit of the camera framerate (30Hz). The experiment has been repeated 3 times for each microrobot. The results of this experiment are the boundary frequencies for all microrobots, and can be found in table III. Using these results, the Rotational Richardson Number (RRN) is calculated as shown in equation 9. This calculation is done for all microrobots, and the results are shown in figure 8.

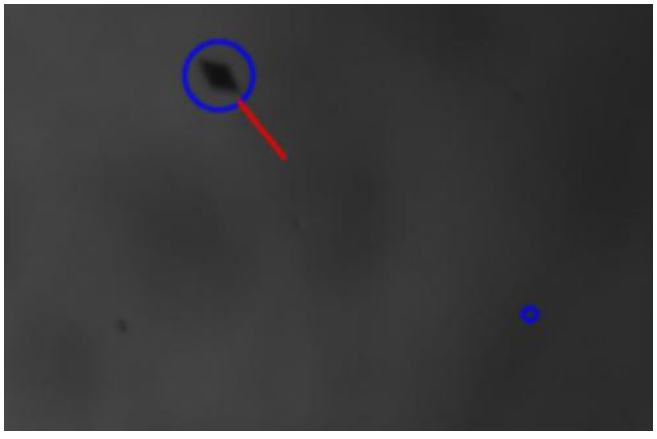

Fig. 7. This figure shows a snapshot of the closed-loop control of a diamond shaped microrobot of 50 × 100 µm. The large circle around the microrobot shows that it is being tracked. The line coming from the microrobot shows the velocity vector. The smaller circle shows the current reference point, to which the microrobot is moving.

B. Linear Velocity Experiments

The linear velocity has been determined for all microrobots. This is done using the maximum magnetic field that we can apply, using 1 A as input current with metal cores in the coils. The position of the microrobot is tracked and used to calculate the velocity. This experiment is repeated 5 times for every microrobot, the results can be found in table II. Using the maximum linear velocity, the Linear Richardson Number (LRN) is calculated as shown in equation 8. This calculation is done for all microrobots, and the results are shown figure 10.

C. Tracking

In order to track the microrobots for experimental work and control a Tracking System was devised using Simulink, which can be seen in figure 9. The tracking works as follows. First a submatrix is taken from the video, this is the area in which the microrobot moves and this is done to shorten calculation time. After this contrast adjustment is applied and erosion to filter out noise. Next, the subsystem is used to create a binary image and dilation is used to enlarge the microrobot. Blob analysis is used to track the microrobots position. The bottom part of the figure is for creating a new video where the microrobot is tracked.

D. Closed-Loop Control

Out of the 6 dimension-groups of microrobots 3 dimensions have been chosen to do closed-loop control. These were the rectangular, ellipsoid and diamond shapes with dimensions 50 × 100 µm, 25 × 250 µm and 50 × 250 µm. These microrobots have been controlled point-to-point in the 2D-setup using an existing controller for microparticles. A typical response of the controlled microrobot can be seen in figure 11. A snapshot of the closed-loop control experiment can be seen in figure 7. The large circle around the microrobot shows that it is being tracked. The line coming from the microrobot shows the velocity vector. The smaller circle shows the current reference point, to which the microrobot is moving.

The closed-loop control experiments have been repeated 5 times on all robots. From these experiments the region of convergence (ROC) has been calculated, which are shown in table IV. The values of the ROC have been plotted as a function of magnetic volume in figure 13. It can be seen from table IV that ROC does not significantly increase when volume increases. In figure 12 a similar graph is made for rotation, the velocity and LRN plotted as function of

TABLE II

AVERAGE LINEAR VELOCITIES MEASURED FOR THE LINEAR PERFORMANCE INDEX EXPERIMENTS.

Linear Velocity measured experimental values ($\mu m/s$)																		
Microrobot	**Rectangle**						**Ellipse**						**Diamond**					
Length (μm)	**100**		**250**		**500**		**100**		**250**		**500**		**100**		**250**		**500**	
Width (μm)	**25**	**50**	**25**	**50**	**25**	**50**	**25**	**50**	**25**	**50**	**25**	**50**	**25**	**50**	**25**	**50**	**25**	**50**
Measurements																		
1	511	633	105	549	471	4308	928	3747	1137	307	387	803	343	1.075	543	3284	353	3571
2	587	839	114	686	601	5069	588	2848	1085	453	429	625	346	1703	142	2434	207	3550
3	551	873	107	581	565	4333	438	2748	1229	495	487	488	297	1842	433	1885	225	3638
Average	**550**	**782**	**109**	**605**	**546**	**4570**	**651**	**3114**	**1150**	**418**	**434**	**639**	**329**	**1540**	**373**	**2534**	**262**	**3586**

TABLE III

BOUNDARY FREQUENCIES MEASURED FOR THE ROTATIONAL PERFORMANCE INDEX EXPERIMENTS.

Boundary Frequency measured experimental values (Hz)																		
Microrobot	**Rectangle**						**Ellipse**						**Diamond**					
Length (μm)	**100**		**250**		**500**		**100**		**250**		**500**		**100**		**250**		**500**	
Width (μm)	**25**	**50**	**25**	**50**	**25**	**50**	**25**	**50**	**25**	**50**	**25**	**50**	**25**	**50**	**25**	**50**	**25**	**50**
Measurements																		
1	4,7	17,4	1,3	7,2	0,4	2,1	12,3	20,4	0,5	11,8	0,4	2,4	3,7	31,9	2,4	9,5	0,4	3,7
2	3,9	16,9	0,8	7,8	0,3	1,9	11,3	19,7	0,3	11,7	0,4	2,8	3,6	31	2,1	9,1	0,4	3,1
3	3,6	16,1	1,1	7,7	0,3	2,1	12,0	19,6	0,5	8,4	0,3	2,7	3,8	30,2	2,0	9,4	0,4	3,1
4	9,1	15,8	1,0	7,5	0,2	2,1	11,8	20,2	0,4	8,4	0,3	2,5	3,3	30,6	2,1	9,5	0,4	3,0
5	5,3	16	1,0	7,4	0,3	1,9	12,0	20,1	0,5	8,4	0,3	2,7	2,4	22,8	1,7	9,7	0,4	3,5
Average	**5,3**	**16,4**	**1,0**	**7,6**	**0,3**	**2,0**	**11,9**	**20**	**0,4**	**9,2**	**0,3**	**2,7**	**3,4**	**29,3**	**2**	**9,4**	**0,4**	**3,2**

volume. Here we see the LRN and controlled velocity depend inversely on magnetic volume.

V. CONCLUSIONS AND FUTURE WORK

First of all we have shown it is possible to control all used microrobots in the 2D setup using maximum magnetic fields of 52.5 mT and maximum gradients of 1.31 T/m. This field and gradient allows us to do point-to-point control with an average region of convergence ranging from 15 µm to 49 µm and velocity ranging from 109 µm/s to 3114 µm/s.

Secondly we can make a statement about the most suitable microrobot for future investigation based on the linear and rotational Richardson number. Both Richardson numbers decrease when magnetic volume increases. This means the smaller microrobots have a larger Richardson number and therewith performance. Looking at the ROC as a function of magnetic material volume we see no trend in increase of the ROC. From this we conclude that the magnetic force on the microrobot is sufficient for control, even for the smallest microrobots. Since the smaller microrobots have more potential for medical applications inside the human body we suggest the smallest ellipsoid, rectangular and diamond shapes are the most suitable for future research.

As a part of future work it is useful to investigate the possibility of getting these or similar microrobots to be self-propelled. This will increase possibilities in medical use since no magnetic field gradients will then be needed for propulsion, These gradients are difficult to generate inside the human body. Other related work is currently being done at this investigating propulsion using a flipping tail on the microrobot. This so called magnetosperm can has a similar structure to the microrobots used in this work. The performance index used and characterization done in this work can be used as an analog to the magnetosperm work.

ACKNOWLEDGMENTS

First of all I would like to thank my daily supervisor Islam Khalil, who was always ready to help me with anything concerning this project. Thank you Sarthak Misra for useful feedback during the weekly meetings and for keeping me on the right track. From the group Transducers Science and Technology, I would like to thank Leon Abelmann for his support and thinking along during the project, Özlem Sardan Sukas for fabricating the microrobots and Laurens Alink for his work on calculating demagnitizing factors. Finally I would like to thank the students of the microrobotics projects for their help and keeping the spirit alive: Roel, Bart, Herman and Marc thanks!

REFERENCES

[1] J. Abbott, Z. Nagy, F. Beyeler and B. Nelson, Robotics in the small, part 1: Microrobotics, *IEEE Robotics and Automation Magazine*, vol. 14, pp. 92-103, June 2007.

[2] B. Nelson, I. Kaliakatsos, J. Abbott, Microrobots for Minimally Invasive Surgery, *Annual Review of Biomedical Engineering*, pp. 55-58, 2010.

[3] H.C. Berg, Random Walks in Biology, *Princeton University Press*, pp. 84, 1993.

[4] A. Nacev, C. Beni, O. Bruno, B Shapiro, Magnetic nanoparticle transport within flowing blood and into surrounding tissue, *PMC Nanomedicine*, pp. 1461, 2010.

[5] M. Bellagia, M. De Graef, On the computation of the demagnetization tensor field for an arbitrary particle shape using a Fourier space approach, *Journal of Magnetism and Magnetic Materials 263*, Volume 263, Issues 12, July 2003

[6] H. Changand J. Burns, Demagnetizing and Stray Fields of Elliptical Films, *Journal of Applied Physics*, Volume 37, July 1966

[7] G.K. Batchelor, An Introduction to Fluid Dynamics, *Cambridge University Press*, Febr 2000

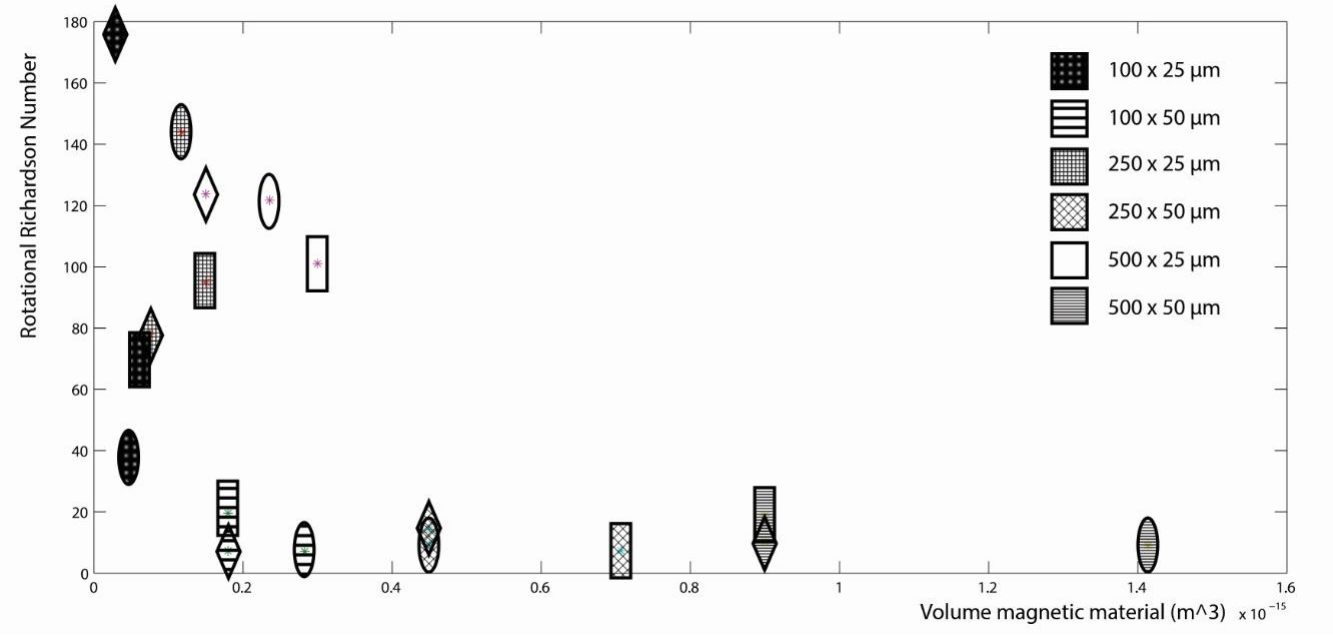

Fig. 8. This graph shows the Rotational Richardson Number versus the volume of the magnetic material for each microrobot. The microrobots are represented by the ellipsoid, rectangular and diamond figures, their filling shows the dimensions of each microrobot. It can be seen that as magnetic material volume increases, the Rotational Richardson Number declines.

TABLE IV

IN THIS TABLE THE REGION OF CONVERGENCE IS SHOWN FOR THE CLOSED-LOOP CONTROL EXPERIMENTS.

Region of Convergence	#1	#2	#3	#4	#5	Average ROC (mm)	STD	%STD
Diamond 100x50	0,035	0,034	0,041	0,034	0,035	**0,036**	0,0028	7,9
Ellipse 100x50	0,042	0,032	0,039	0,035	0,040	**0,038**	0,0042	11,1
Rectangle 100x50	0,026	0,026	0,026	0,023	0,023	**0,025**	0,0016	6,7
Diamond 250x25	0,015	0,013	0,010	0,018	0,018	**0,015**	0,0034	22,7
Ellipse 250x25	0,018	0,025	0,016	0,028	0,030	**0,023**	0,0060	25,7
Rectangle 250x25	0,042	0,055	0,049	0,052	0,048	**0,049**	0,0053	10,7
Diamond 250x50	0,029	0,033	0,036	0,032	0,033	**0,033**	0,0025	7,5
Ellipse 250x50	0,018	0,025	0,013	0,024	0,030	**0,022**	0,0063	28,9
Rectangle 250x50	0,047	0,059	0,045	0,044	0,033	**0,046**	0,0095	20,8

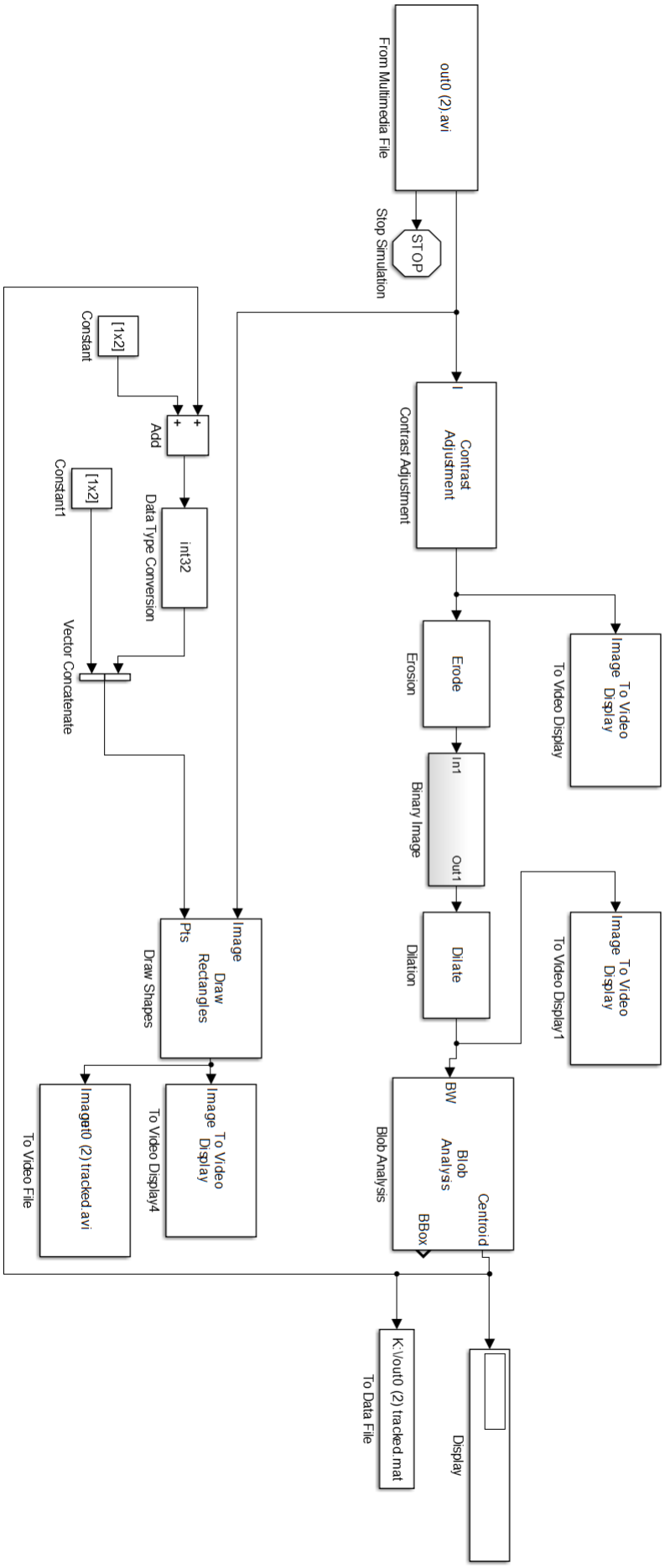

Fig. 9. In this figure the tracking system is shown. The video is imported and a submatrix is applied. After this contrast adjustment is done. After erosion a subsystem is applied to create a binary image. After dilation blob analyses is used to find the position of the microrobot. The bottom part of the figure is used to create a new video where the microrobot is tracked and this is visualised.

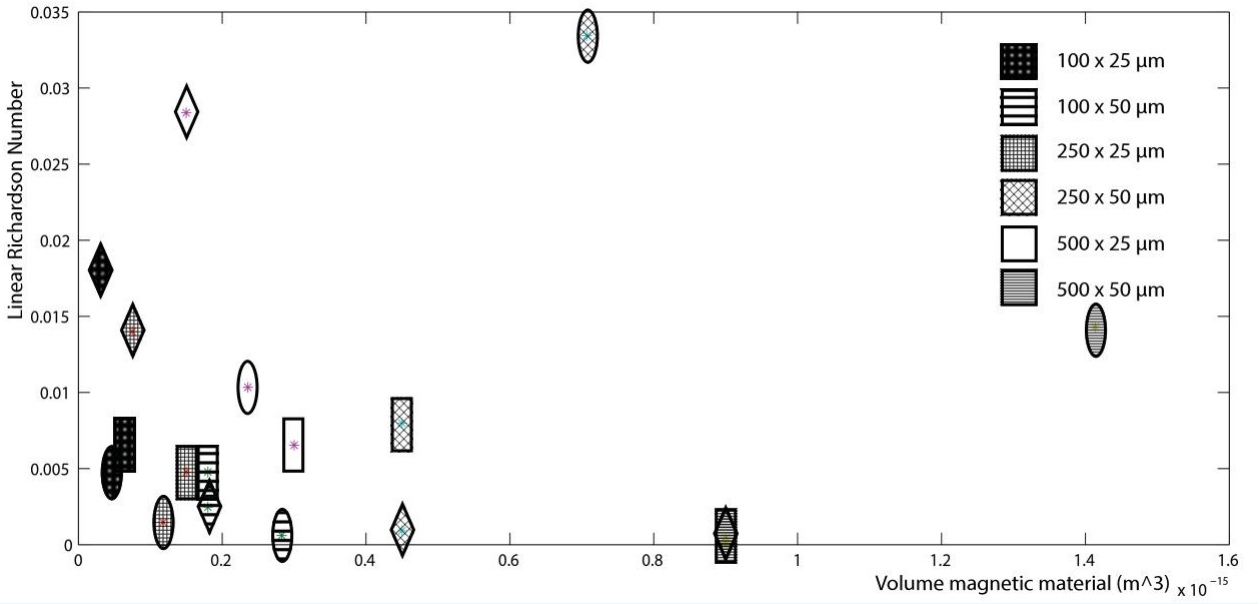

Fig. 10. This graph shows the Linear Richardson Number versus the volume of the magnetic material for each microrobot. The microrobots are represented by the ellipsoid, rectangular and diamond figures, their filling shows the dimensions of each microrobot. It can be seen that as magnetic material volume increases, the Linear Richardson Number declines.

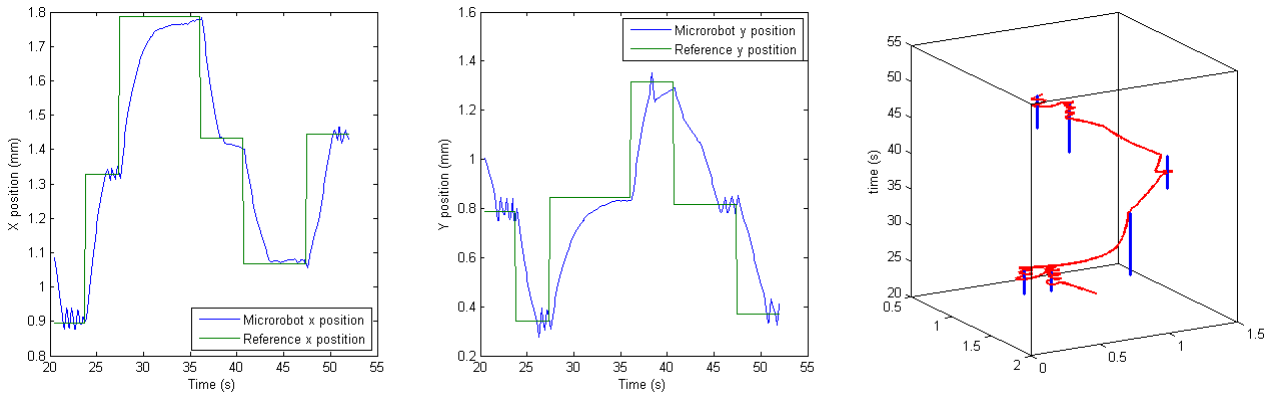

Fig. 11. Response of the diamond shaped 50 × 100 µm microrobot to closed-loop point-to-point control. In the first graph the x position of the microrobot is shown, in the second the y position and in the third a 3D-image of microrobot position in time.

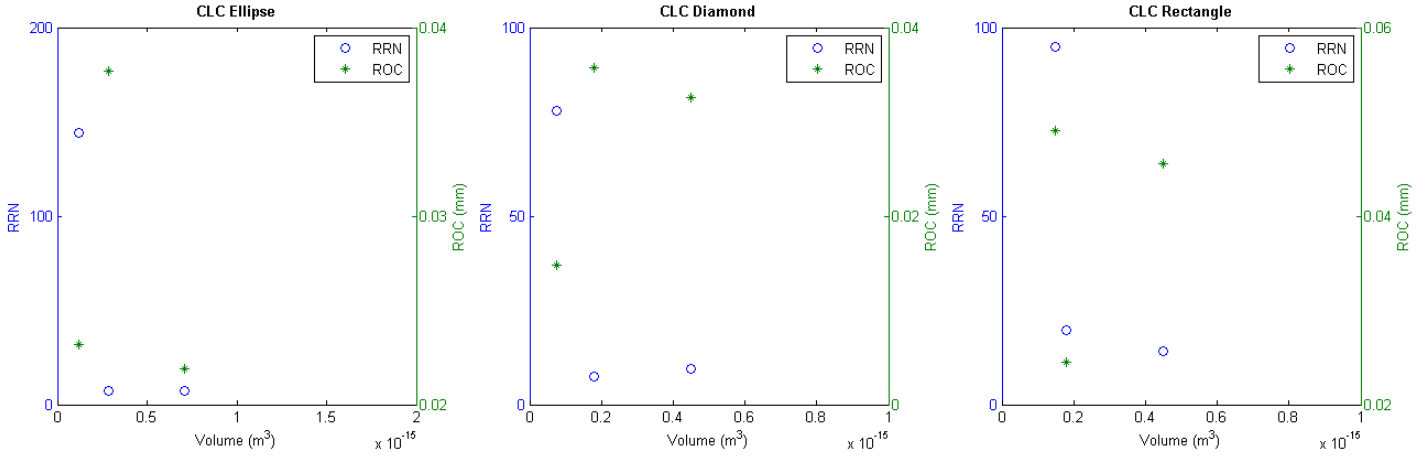

Fig. 12. This graphs show the Rotational Richardson Number and velocity as a function of magnetic material volume.

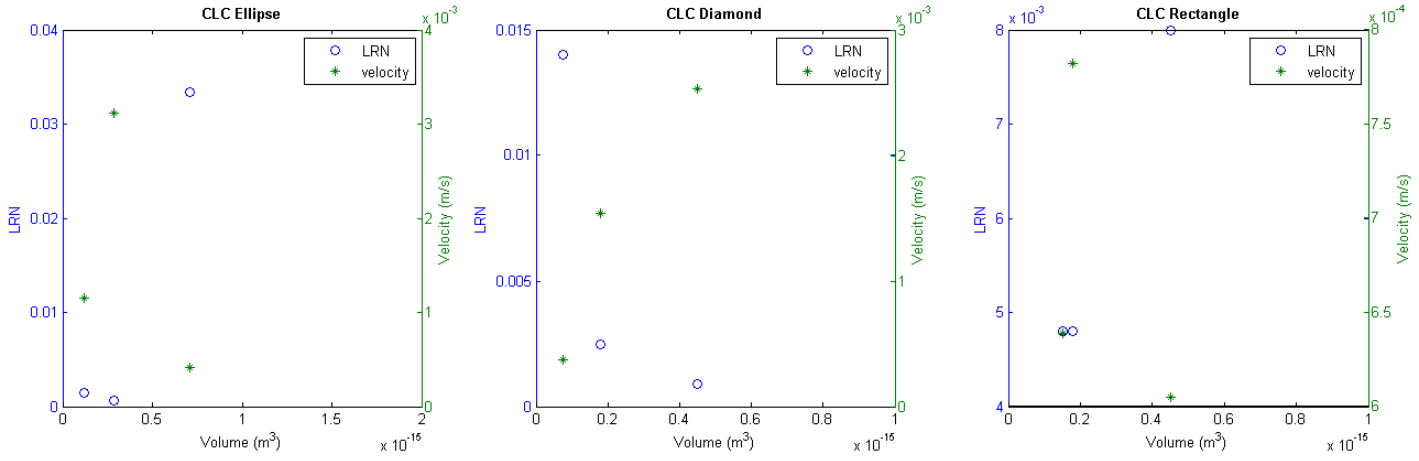

Fig. 13. This graphs show the Linear Richardson Number and Region of Convergence as a function of magnetic material volume.